

## A statistical model of turbulence in two-dimensional mixing layers

By CHRISTOPHER K. W. TAM AND K. C. CHEN

Department of Mathematics, Florida State University, Tallahassee

(Received 10 April 1978)

A statistical model based on the proposition that the turbulence of a fully developed two-dimensional incompressible mixing layer is in a state of quasi-equilibrium is developed. In this model the large structures observed by Brown & Roshko (1974) which will be assumed to persist into the fully developed turbulent region are represented by a superposition of the normal wave modes of the flow with arbitrary random amplitudes. The turbulence at a point in the flow is assumed to be dominated by the fluctuations associated with these large structures. These structures grow and amalgamate as they are convected in the flow direction. Because of the lack of intrinsic length and time scales the turbulence in question can, therefore, be regarded as created or initiated at an upstream point, the virtual origin of the mixing layer, by turbulence with a white noise spectrum and are subsequently convected downstream. The model is used to predict the second-order turbulence statistics of the flow including single point turbulent Reynolds stress distribution, intensity of turbulent velocity components, root-mean-square turbulent pressure fluctuations, power spectra and two-point space-time correlation functions. Numerical results based on the proposed model compare favourably with available experimental measurements. Predictions of physical quantities not yet measured by experiments, e.g. the root-mean-square pressure distribution across the mixing layer, are also made. This permits the present model to be further tested experimentally.

---

### 1. Introduction

In this paper a statistical model of turbulence in fully developed two-dimensional incompressible turbulent mixing layers is proposed. The development of this model is largely motivated by the recent experimental observations of Brown & Roshko (1974). They found that in this class of flows the turbulence field consists of many large vortex-like structures. The sizes of these structures are of the order of the local mixing layer thickness. The dynamics of the large vortex-like structures is governed by the processes of convective amplification (the large structures grow as they are being convected downstream) and amalgamation. The former process infers that the turbulence state at any cross-section of the mixing layer downstream can be considered as being excited or created at an upstream point and then convected to the point in question. The latter process assures that the turbulent fluctuation at any point is stochastic or random. These two important observations suggest that perhaps the state of turbulence at any cross-section in a fully developed two-dimensional turbulent

mixing layer can be regarded as initiated upstream by turbulence with a completely random white noise spectrum. The reason that the upstream spectrum should have white noise characteristics is that for sufficiently high Reynolds number flow the problem has no intrinsic length and time scales. The lack of intrinsic length and time scales renders the two-dimensional mixing layer flow and all its turbulence statistics similar. Physically, similarity implies that the flow is in a dynamical quasi-equilibrium state. So a statistical model patterned after the approach of classical statistical mechanics becomes attractive and feasible. To implement this idea it will be assumed that in terms of a set of dimensionless similarity co-ordinate variables formed by using the local mixing layer thickness as the length scale, the fluctuations associated with the large structures which dominate the turbulence field can be represented by a superposition of the normal modes (hydrodynamic wave modes) of the flow. This interpretation of flow similarity and the two key observations of Brown & Roshko (1974) form the basis of our proposed statistical model. The formulation of this model is described in detail in § 2 below.

In the past a number of theories of turbulence based on hydrodynamic stability solutions of the mean flow profile have been proposed by various authors. However, a closer examination reveals that the basic premise and formulation of these theories differ completely from the present model. The first theory of this kind was proposed by Malkus (1956) who studied the turbulent shear flow between two parallel plates. In his theory the marginally stable waves were singled out among all the wave modes. These marginally stable waves played a crucial role in determining the mean velocity profile in his analysis. Subsequently, the turbulence in a boundary layer was investigated by Landahl (1967, 1975) and Bark (1975) using a wave-guide model. It was shown that in this case all the small amplitude waves were damped. In Landahl's work the least damped waves were assumed to dominate over the other kinds of disturbances. So that by determining the decay rate and convection velocity of these waves numerically Landahl was able to estimate the corresponding quantities of the turbulence field of a flat-plate boundary layer. In contrast to the parallel plates and the boundary-layer problems the present two-dimensional mixing layers are known to possess unstable mean velocity profiles. As a result, the unstable spectrum is most important in the proposed model. Although stability waves or normal modes of the flow are used in our formulation, they are only to be regarded as a convenient way of representing the wave decomposition of the large structures. On the other hand, waves of this kind in turbulent free shear flows have recently been observed by Chan (1974*a, b*, 1976, 1977) and Moore (1977). They found that the gross properties of these waves agreed quite well with the prediction of locally parallel flow stability analysis. Thus these experiments actually provide a physical basis to an otherwise purely mathematical representation of the turbulent large structures in the mixing layer.

The main objective of this work is to predict the second-order turbulence statistics of two-dimensional fully developed turbulent mixing layers. These statistics include turbulent Reynolds stress, intensities of turbulent velocity components, distribution of root-mean-square pressure fluctuations, power spectra and two-point space-time correlation functions. Not all these quantities have been measured in the past so that some of the predictions of this work can actually be verified or disproved experimentally. In § 4 numerical results of the present model are used to compare with available experimental measurements. Favourable overall agreements are found

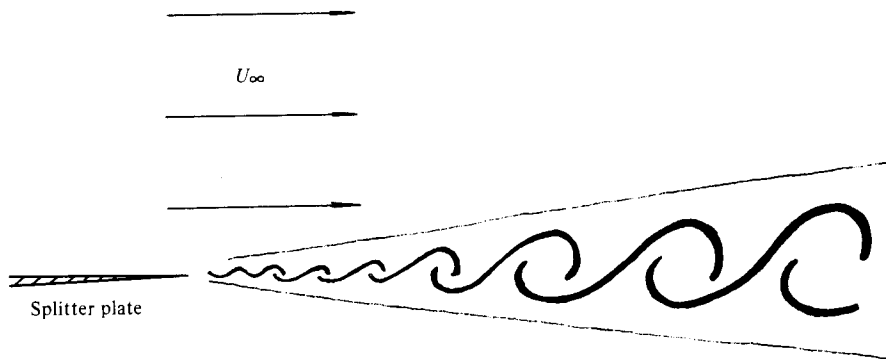


FIGURE 1. A stretch of large structures in a two-dimensional mixing layer.

lending support to the general validity of the proposed statistical model. Further discussions of this model in relation to laboratory experimental measurements and other turbulence transport theories are given at the end of this paper.

## 2. Formulation

Before we present our proposed statistical model of turbulence in two-dimensional mixing layers we will first review some of the most pertinent experimental findings of the last few years which in many ways have radically changed our concept of turbulence in this class of flows. Contrary to the classical notion of turbulence, recent experimental observations of Brown & Roshko (1974), Roshko (1976), Dimotakis & Brown (1976) revealed that turbulence in two-dimensional mixing layers is far more orderly than had previously been believed. The turbulence field is found to be dominated by large vortex-like structures, see figure 1. Motion pictures taken by Brown & Roshko indicate that these large structures are initiated near the trailing edge of the splitter plate which marks the beginning of the mixing layer. These structures grow in size as they are convected downstream. To accommodate this growth the spacings between neighbouring structures undergo constant changes. Every now and then two (or three) of these vortex-like structures would coalesce to form a single larger structure. This process, which was observed to occur more prominently at low Reynolds number by Winant & Browand (1974), is generally referred to as 'vortex pairing' (or tripling). In high Reynolds number flows the pairing process once started is usually completed in very short intervals of time. In addition to the pairing phenomenon Dimotakis & Brown (1976) observed that a large structure may abruptly disintegrate in the straining field of the adjacent large structure (or structures). When this takes place the fluid associated with the disintegrated structure then becomes a part of the collective motion of the neighbouring structure (or structures). They called this process of amalgamation 'tearing'. Acting together the mechanisms of 'vortex pairing' and 'tearing' are instrumental in randomizing the space-time trajectories of the large structures. Thus although a single large structure may appear as quasi-deterministic the sum total of all the large structures in the mixing layer amalgamating randomly in space and time gives the overall phenomenon a stochastic and chaotic character typical of turbulent flows. As far as is known the surviving large structures have extremely long lifetimes. In all the experiments mentioned above they seemed to

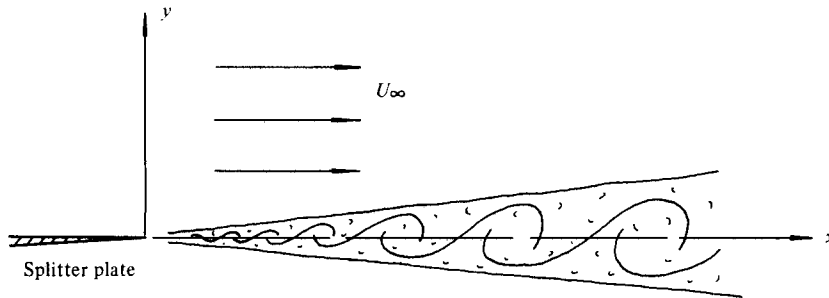


FIGURE 2. Idealized two-dimensional incompressible fully developed turbulent mixing layer with no intrinsic length and time scales.

persist all the way to the end of the testing sections. On the basis of this fact it is believed that the large structures actually constitute the dominant part of the turbulence field in what was previously known as fully developed turbulent mixing layers.

### 2.1. A quasi-equilibrium statistical model

We will now restrict our attention to an idealized two-dimensional incompressible mixing layer which is in a fully developed turbulent state as shown in figure 2. We will neglect the boundary layer on the splitter plate so that the mixing layer begins at a point, viz. the trailing edge of the splitter plate (one can consider this to be the virtual origin of a fully developed turbulent mixing layer). In this work our objective is not to describe the quasi-deterministic behaviour of the large structures of the turbulence. Rather, our aim is to develop a statistical model capable of predicting the second-order turbulence statistics of the flow. These include single point statistics such as the turbulence Reynolds stress,  $\langle uv \rangle$ , turbulent kinetic energy components,  $\langle u^2 \rangle$ ,  $\langle v^2 \rangle$  and  $\langle w^2 \rangle$ , pressure fluctuations  $\langle p^2 \rangle$ , power spectrum  $\langle u^2(f) \rangle$  etc. and two-point space-time correlation functions ( $\langle \rangle =$  ensemble average). In developing the present model explicit reference to individual vortex-like large structure and its motion will not be made. Here only the collective behaviour of all the large structures in the mixing layer is of importance in calculating statistical averages. For this purpose we will describe the large structures by wave representation (decomposition of the large structures into appropriate wave components). The use of a wave representation is not simply only a matter of mathematical convenience; it can be partly justified on physical grounds. Dimotakis & Brown (1976) have demonstrated that the large structures in a mixing layer are strongly coupled or locked to each other even for those that are very far apart. This long range interaction causes the overall motion of the row of large structures to be wave-like although individually the internal motion of a single structure may be vortex-like. Since we will not be interested in a single large structure alone the use of a wave decomposition to describe the motion of the large structures is, therefore, quite appropriate.

The following two hypotheses will be used in formulating our statistical model.

(1) Only flow fluctuations associated with the large structures are considered important in determining second-order turbulence statistics.

(2) The flow is similar.

Both hypotheses are supported by experimental evidence. The first hypothesis needs

no further elaboration as it is the subject of many recent works; some of which have been discussed above. Chandrsuda *et al.* (1978) recently suggested that under normal laboratory conditions (without taking extreme precaution in eliminating external disturbances) the large structures in fully developed turbulent mixing layers might be less orderly than those observed by Brown & Roshko (1974). However they do believe that the large structures are the dominant elements of the turbulence field. The second hypothesis is rooted in the observation that the idealized problem (see figure 2) has no intrinsic length and time scales when the flow Reynolds number is very large. Because of the lack of intrinsic length scale all the ensemble-averaged physical quantities of the problem which have a length dimension must vary like  $x$ , the distance measured downstream from the initial point of the two-dimensional mixing layer, or the local thickness,  $\delta$ , of the shear layer. The local thickness  $\delta = x/\sigma$ , where  $\sigma$  is the spreading parameter, is a slowly varying function of  $x$ . In addition, all the variables with dimension of time must vary like  $x/U_\infty$  or  $\delta/U_\infty$  where  $U_\infty$  is the free-stream velocity. Similarity applies not only to the mean flow profile alone but to all ensemble-averaged turbulence statistics (second- and all higher-order statistics) as well. To demonstrate the existence of similarity in turbulence statistics extensive and laborious experimental measurements are necessary. As a result of the enormous amount of effort needed, available experimental data are generally confined to only a few single point second-order statistics. They can be found in the works of Liepmann & Laufer (1947), Wygnanski & Fiedler (1970), Patel (1973), Champagne, Pao & Wygnanski (1976); most of these data do support the similarity argument. Figure 3 shows the normalized longitudinal turbulent velocity power spectrum

$$\langle u^2(S) \rangle / \int_0^\infty \langle u^2(S) \rangle dS$$

(where  $S = fx/U_\infty$  is the Strouhal number and  $f$  is the frequency) at various axial distances downstream of the nozzle exit in the initial mixing layer of a 3.5 in. diameter jet measured by Laurence (1956). The flow Mach number was 0.3 and the data were taken along a line at approximately one radius from the centre-line of the jet. As can be seen, with  $x/U_\infty$  as the time scale a reasonably good collapse of the power spectra data is obtained indicating that the turbulent shear layer flow is quite similar.

Physically, similarity implies that the turbulent fluctuations are in a state of quasi-equilibrium. This can be visualized by following the flow as it moves downstream. Since the change in local thickness  $\delta$  of the shear layer is very slow and all the statistical averages of the state of the turbulent flow are scaled according to  $\delta$  they are effectively constants (at least locally). To the order of approximation that the rate of change of  $\delta$ , i.e.  $d\delta/dx = 1/\sigma \ll 1$ , is negligible the flow is essentially stationary with respect to time as the flow moves downstream and hence it is in statistical quasi-equilibrium. For systems which are in equilibrium such as a gas at thermal equilibrium or phonons in black body radiation problems, classical statistical methods can be applied to determine some of the gross properties of the systems. One of the attractive features of these statistical approaches is that the detailed interaction between the numerous components which make up the system need not be known. In the present case if a similar statistical method is used, a detailed understanding of the nonlinear interaction between different scale components of turbulence could probably be avoided. This is the key factor of the present statistical model. Making an analogy to the problem

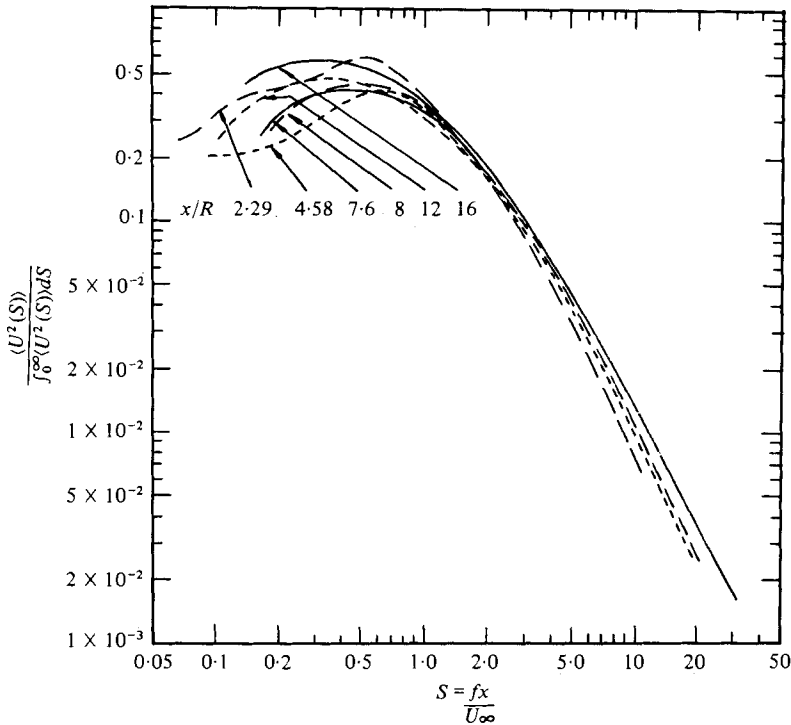


FIGURE 3. Normalized longitudinal turbulent spectra at various axial distances downstream of the nozzle exit of a 3.5 in. diameter jet at approximately one radius from the centre-line. Flow Mach number is 0.3. Data taken from Laurence (1956).

of black body radiation from a cavity at thermal equilibrium, we will assume that the turbulent fluctuations  $u, v, w$  (velocity components) and  $p$  (pressure) can be represented by a linear combination of the normal wave modes of the flow. The amplitudes of the modes are, however, considered as stochastic random functions. That is:

$$\text{turbulent fluctuations} = \sum_i a_i \cdot (\textit{i} \text{th normal mode of the flow}), \quad (2.1)$$

where  $a_i$  is a random function. A more precise statement of this normal mode representation will be given later.

Similarity also implies that the state of turbulence has no memory of its past history. In fact, it does not matter whether the flow begins with a laminar or turbulent initial condition, the characteristics of the fully developed turbulent region are the same. In a turbulent flow the nonlinear process of 'vortex pairing' and 'tearing' completely randomize the large structures and as a result cause the flow to attain an asymptotic similarity state. The lack of dependence on initial conditions is extremely important for the turbulence can now be regarded as generated by a completely random initial excitation having no characteristic length and time scales. This provides a constraint on the turbulence spectrum or the random wave amplitudes of the normal modes of the flow. Mathematically, in conjunction with the wave representation of the turbulence field adopted above this condition can be stated as follows. The wave spectrum of the turbulent state at any position downstream (see

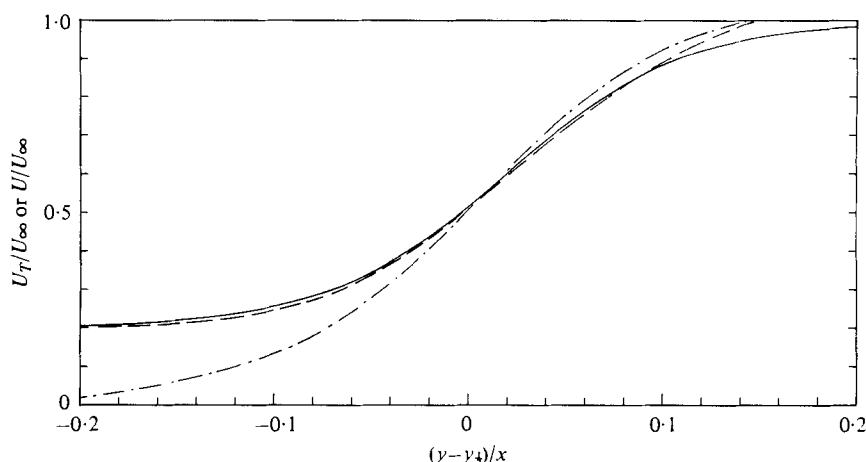


FIGURE 4. Temporal and conditional turbulent mean velocity profile as measured by Wygnanski & Fiedler (1970). ---, mean velocity profile,  $U/U_\infty$ ; -·-, conditional turbulent mean velocity profile,  $U_T/U_\infty$ ; —, equation (2.3),  $\eta = \sigma(y - y_1)/x - 0.22$ ,  $y_1 =$  location where  $U/U_\infty$  is 0.5.

figure 2) can be considered to be initiated by a completely random excitation at the virtual origin of the mixing layer. In terms of the correlation function of the turbulent velocity components at the virtual origin this can be expressed as

$$\frac{1}{U_\infty^2} \langle u(z, t) u(z + \zeta, t + \tau) + v(z, t) v(z + \zeta, t + \tau) + w(z, t) w(z + \zeta, t + \tau) \rangle = 4\pi^2 \tilde{R}(\zeta) \delta(\tau), \tag{2.2}$$

where  $\delta(\zeta)$  and  $\delta(\tau)$  are Dirac delta-functions and  $\tilde{R}$  is the area of the autocorrelation function;  $\langle \rangle =$  ensemble average.

To sum up, our statistical model of turbulence consists of representing the turbulent fluctuations by the normal modes of the flow with random amplitudes. The distribution of the amplitudes is to be determined by the condition that the turbulent wave spectrum at any downstream location could be considered as generated by an initial spectrum whose kinetic energy has no intrinsic length or time scales, namely, a white noise spectrum. The last statement is equivalent to requiring its autocorrelation function to have delta function characteristics.

### 2.2. Normal mode representation

We will represent the large structures of the mixing layer by linear combination of the hydrodynamic stability modes of the flow. They are given by the eigensolutions of the Orr-Sommerfeld equation. However, we like to point out that we are not interested in analysing the stability of the mean flow. Our objective is to find a simple way to best represent the large structures. In the mixing layer the temporal mean flow is certainly not the mean flow as seen by the large structures. We believe that the conditional turbulent mean flow profile is probably a much better approximation for our purpose and will, therefore, be used in all subsequent analysis and computation. Figure 4 shows the conditional turbulent mean flow profile,  $U_T/U_\infty$ , as measured by Wygnanski & Fiedler (1970). A reasonably good fit to the measured data in terms of simple analytic functions is

$$(U_T/U_\infty) = 0.6 + 0.4 \tanh \eta, \tag{2.3a}$$

where  $\eta = y/\delta + \eta_0, \quad \delta = x/\sigma, \quad \sigma = 11, \quad \eta_0 = 0.08. \tag{2.3b}$

The linearized equations of motion with  $(U_T, 0, 0)$  as the mean flow are:

$$\frac{\partial u}{\partial x} + \frac{\partial v}{\partial y} + \frac{\partial w}{\partial z} = 0; \quad (2.4a)$$

$$\frac{\partial u}{\partial t} + U_T \frac{\partial u}{\partial x} + v \frac{\partial U_T}{\partial y} = -\frac{1}{\rho} \frac{\partial p}{\partial x} + \nu_T \nabla^2 u; \quad (2.4b)$$

$$\frac{\partial v}{\partial t} + U_T \frac{\partial v}{\partial x} = -\frac{1}{\rho} \frac{\partial p}{\partial y} + \nu_T \nabla^2 v; \quad (2.4c)$$

$$\frac{\partial w}{\partial t} + U_T \frac{\partial w}{\partial x} = -\frac{1}{\rho} \frac{\partial p}{\partial z} + \nu_T \nabla^2 w; \quad (2.4d)$$

where  $\nu_T$  is a turbulent eddy viscosity provided by the fine scale turbulence of the flow. We will delay the discussion on  $\nu_T$  and its appropriateness to a later section. Let the Fourier transform of a function  $\phi$  in  $z$  and  $t$  be denoted by  $\check{\phi}'$ . The Fourier transform pair  $\phi$  and  $\check{\phi}'$  are related by

$$\phi(x, y, z, t) = \iint_{-\infty}^{\infty} \check{\phi}'(x, y, \alpha, \omega) \exp[i(\alpha z - \omega t)] d\alpha d\omega, \quad (2.5a)$$

$$\check{\phi}'(x, y, \alpha, \omega) = \frac{1}{(2\pi)^2} \iint_{-\infty}^{\infty} \phi(x, y, z, t) \exp[-i(\alpha z - \omega t)] dz dt. \quad (2.5b)$$

The Fourier transforms of equations (2.4) are:

$$\frac{\partial \check{u}'}{\partial x} + \frac{\partial \check{v}'}{\partial y} + i\alpha \check{w}' = 0; \quad (2.6a)$$

$$-i\omega \check{u}' + U_T \frac{\partial \check{u}'}{\partial x} + \check{v}' \frac{\partial U_T}{\partial y} = -\frac{1}{\rho} \frac{\partial \check{p}'}{\partial x} + \nu_T \left( \frac{\partial^2 \check{u}'}{\partial x^2} + \frac{\partial^2 \check{u}'}{\partial y^2} - \alpha^2 \check{u}' \right); \quad (2.6b)$$

$$-i\omega \check{v}' + U_T \frac{\partial \check{v}'}{\partial x} = -\frac{1}{\rho} \frac{\partial \check{p}'}{\partial y} + \nu_T \left( \frac{\partial^2 \check{v}'}{\partial x^2} + \frac{\partial^2 \check{v}'}{\partial y^2} - \alpha^2 \check{v}' \right); \quad (2.6c)$$

$$-i\omega \check{w}' + U_T \frac{\partial \check{w}'}{\partial x} = -\frac{i\alpha}{\rho} \check{p}' + \nu_T \left( \frac{\partial^2 \check{w}'}{\partial x^2} + \frac{\partial^2 \check{w}'}{\partial y^2} - \alpha^2 \check{w}' \right). \quad (2.6d)$$

Now fundamental to the assumption of our quasi-equilibrium model is that the spatial rate of change in  $\delta$  is negligible. Therefore, by regarding  $\delta$  as a constant (at least locally), (2.6) can be rewritten in terms of the following similarity co-ordinate variables.

$$\xi = x/\delta, \quad \eta = y/\delta + \eta_0. \quad (2.7)$$

These similarity variables effectively transform the slowly divergent turbulent mixing layer into a parallel flow. This is illustrated in figure 5. The use of similarity co-ordinate variables  $(\xi, \eta)$  is important for it is in the  $\xi, \eta$  plane that the turbulent flow is stationary random. Now (2.6) can be put into a dimensionless form using the following variables,

$$\left. \begin{aligned} \tilde{u} &= \check{u}'/U_\infty, & \tilde{v} &= \check{v}'/U_\infty, & \tilde{w} &= \check{w}'/U_\infty, & \tilde{p} &= \check{p}'/\rho U_\infty^2, \\ \bar{w} &= \frac{\omega \delta}{U_\infty}, & \bar{\alpha} &= \alpha \delta, & R_T &= \frac{U_\infty \delta}{\nu_T}, & \bar{U}_T &= \frac{U_T}{U_\infty}. \end{aligned} \right\} \quad (2.8)$$

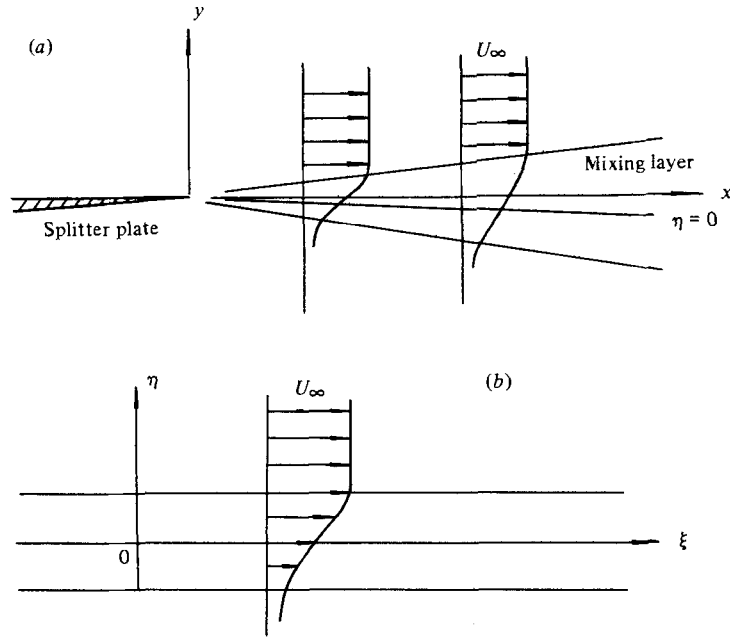


FIGURE 5. Mapping of the mixing layer into the  $\xi, \eta$  plane where the turbulence is stationary random. (a) Physical co-ordinates. (b) Similarity co-ordinates.

$$\frac{\partial \tilde{u}}{\partial \xi} + \frac{\partial \tilde{v}}{\partial \eta} + i\bar{\alpha}\tilde{w} = 0; \tag{2.9a}$$

$$-i\bar{\omega}\tilde{u} + \bar{U}_T \frac{\partial \tilde{u}}{\partial \xi} + \tilde{v} \frac{d\bar{U}_T}{d\eta} = -\frac{\partial \tilde{p}}{\partial \xi} + \frac{1}{R_T} \left( \frac{\partial^2 \tilde{u}}{\partial \xi^2} + \frac{\partial^2 \tilde{u}}{\partial \eta^2} - \bar{\alpha}^2 \tilde{u} \right); \tag{2.9b}$$

$$-i\bar{\omega}\tilde{v} + \bar{U}_T \frac{\partial \tilde{v}}{\partial \xi} = -\frac{\partial \tilde{p}}{\partial \eta} + \frac{1}{R_T} \left( \frac{\partial^2 \tilde{v}}{\partial \xi^2} + \frac{\partial^2 \tilde{v}}{\partial \eta^2} - \bar{\alpha}^2 \tilde{v} \right); \tag{2.9c}$$

$$-i\bar{\omega}\tilde{w} + \bar{U}_T \frac{\partial \tilde{w}}{\partial \xi} = -i\bar{\alpha}\tilde{p} + \frac{1}{R_T} \left( \frac{\partial^2 \tilde{w}}{\partial \xi^2} + \frac{\partial^2 \tilde{w}}{\partial \eta^2} - \bar{\alpha}^2 \tilde{w} \right). \tag{2.9d}$$

We will now look for separable wave-like solutions of equation (2.9) of the form

$$\left. \begin{aligned} \tilde{u} &= \hat{u}(\eta, \bar{\alpha}, \bar{\omega}) e^{ik\xi}, \\ \tilde{v} &= \hat{v}(\eta, \bar{\alpha}, \bar{\omega}) e^{ik\xi}, \\ \tilde{w} &= \hat{w}(\eta, \bar{\alpha}, \bar{\omega}) e^{ik\xi}, \\ \tilde{p} &= \hat{p}(\eta, \bar{\alpha}, \bar{\omega}) e^{ik\xi}. \end{aligned} \right\} \tag{2.10}$$

and

Upon substitution of (2.10) into equation (2.9) and elimination of all other variables we obtain the familiar Orr-Sommerfeld equation for  $\hat{v}$  except that the conditional turbulent mean velocity profile is to be used,

$$\left( \frac{d^2}{d\eta^2} - \bar{\alpha}^2 - k^2 \right)^2 \hat{v} - iR_T \left[ (k\bar{U}_T - \bar{\omega}) \left( \frac{d^2}{d\eta^2} - \bar{\alpha}^2 - k^2 \right) \hat{v} - k\bar{U}_T'' \hat{v} \right] = 0. \tag{2.11}$$

The appropriate boundary conditions are

$$\hat{v} \rightarrow 0 \quad \text{as} \quad \eta \rightarrow \pm \infty. \tag{2.12}$$

For given real values of  $\bar{\omega}$  and  $\bar{\alpha}$  equation (2.11) and boundary condition (2.12) form an eigenvalue problem by which the complex eigenvalue  $k = k_r + ik_i$  ( $k_r$  and  $k_i$  are the real and imaginary parts of  $k$ ) is determined. In the appendix it is proven that the eigenvalues and the corresponding eigenfunctions  $\hat{v}$ ,  $\hat{u}$ ,  $\hat{w}$  and  $\hat{p}$  possess a number of important properties.

(i) The eigenvalues and eigenfunctions are invariant to the transformation  $\bar{\alpha} \rightarrow -\bar{\alpha}$ .

(ii) If  $k = k_r(\bar{\alpha}, \bar{\omega}) + ik_i(\bar{\alpha}, \bar{\omega})$  is an eigenvalue, then  $k(\bar{\alpha}, -\bar{\omega})$  is also an eigenvalue. It is related to  $k(\bar{\alpha}, \bar{\omega})$  by the relation

$$k(\bar{\alpha}, -\bar{\omega}) = -k^*(\bar{\alpha}, \bar{\omega}), \quad (2.13)$$

where \* denotes the complex conjugate.

(iii) When properly normalized the eigenfunction corresponding to  $(\bar{\alpha}, -\bar{\omega})$  is the complex conjugate of that of  $(\bar{\alpha}, \bar{\omega})$ , i.e.

$$\hat{v}^*(\eta, \bar{\alpha}, \bar{\omega}) = \hat{v}(\eta, \bar{\alpha}, -\bar{\omega}). \quad (2.14)$$

Since  $\hat{v}$  is a complex function we can adopt two real normalization conditions. To ensure that equation (2.14) holds we will require that

$$\hat{v}(0, \bar{\alpha}, \bar{\omega}) = \hat{v}(0, \bar{\alpha}, -\bar{\omega}), \quad (2.15a)$$

that is they are real and equal. In addition, for convenience, we will normalize the eigenfunctions so that at  $\eta = 0$  the sum of the squares of the absolute values of  $\hat{u}$ ,  $\hat{v}$ , and  $\hat{w}$  is equal to unity:

$$|\hat{u}(0, \bar{\alpha}, \bar{\omega})|^2 + |\hat{v}(0, \bar{\alpha}, \bar{\omega})|^2 + |\hat{w}(0, \bar{\alpha}, \bar{\omega})|^2 = 1. \quad (2.15b)$$

After the eigenvalue  $k$  and eigenfunction  $\hat{v}$  are found and the latter properly normalized, the pressure  $\hat{p}$  is computed according to the formula

$$\hat{p} = \frac{1}{k^2 + \bar{\alpha}^2} \left\{ \frac{1}{R_T} \left[ \frac{d^3 \hat{v}}{d\eta^3} - (k^2 + \bar{\alpha}^2) \frac{d\hat{v}}{d\eta} \right] + i(\bar{\omega} - \bar{U}_T k) \frac{d\hat{v}}{d\eta} + ik \frac{d\bar{U}_T}{d\eta} \hat{v} \right\}. \quad (2.16)$$

Equation (2.16) can easily be derived from (2.9) by eliminating  $\hat{u}$  and  $\hat{w}$ . The longitudinal and lateral velocity components  $\hat{u}$  and  $\hat{w}$  cannot be obtained explicitly in terms of  $\hat{v}$ ,  $\hat{p}$  and their derivatives. They are to be found by integrating the inhomogeneous equations (2.9b) and (2.9d) with the boundary conditions  $\hat{u}, \hat{w} \rightarrow 0$  as  $\eta \rightarrow \pm \infty$ .

The eigenvalue problem (2.11) and (2.12) has been studied by many authors in the past. It has been found that for a mean velocity profile typical of that given by equation (2.3a) there is only one family of unstable eigensolutions. It can be shown that only the unstable wave components contribute significantly to the second-order statistics of the flow turbulence. Thus for simplicity we will only consider the contribution of this family of eigensolutions. Let  $a(\alpha, \omega)$  be the stochastic random amplitude function of the unstable wave mode. Then by Fourier inverse transforms the turbulent velocity and pressure fluctuations in the mixing layer will be given by:

$$\begin{aligned} \frac{u(\xi, \eta, z, t)}{U_\infty} &= \iint_{-\infty}^{\infty} a(\alpha, \omega) \frac{\delta}{U_\infty^{\frac{1}{2}}} \hat{u}(\eta, \bar{\alpha}, \bar{\omega}) \exp[i(k\xi + \alpha z - \omega t)] d\alpha d\omega; \\ \frac{v(\xi, \eta, z, t)}{U_\infty} &= \iint_{-\infty}^{\infty} a(\alpha, \omega) \frac{\delta}{U_\infty^{\frac{1}{2}}} \hat{v}(\eta, \bar{\alpha}, \bar{\omega}) \exp[i(k\xi + \alpha z - \omega t)] d\alpha d\omega; \\ \frac{w(\xi, \eta, z, t)}{U_\infty} &= \iint_{-\infty}^{\infty} a(\alpha, \omega) \frac{\delta}{U_\infty^{\frac{1}{2}}} \hat{w}(\eta, \bar{\alpha}, \bar{\omega}) \exp[i(k\xi + \alpha z - \omega t)] d\alpha d\omega; \\ \frac{p(\xi, \eta, z, t)}{\rho U_\infty^2} &= \iint_{-\infty}^{\infty} a(\alpha, \omega) \frac{\delta}{U_\infty^{\frac{1}{2}}} \hat{p}(\eta, \bar{\alpha}, \bar{\omega}) \exp[i(k\xi + \alpha z - \omega t)] d\alpha d\omega. \end{aligned} \quad (2.17)$$

2.3. Properties of random amplitude function  $a(\alpha, \omega)$

To complete the formulation of our statistical model we will proceed to find the stochastic properties of the random amplitude function  $a(\alpha, \omega)$ . This is done by invoking (2.2) which requires that the turbulence at any location downstream of the trailing edge of the splitter plate can be regarded as generated by turbulent excitations at the virtual origin of the mixing layer, i.e. the origin of the similarity plane  $\xi = \eta = 0$  (see figure 5). The autocorrelation function of the turbulent kinetic energy at the virtual origin has no characteristic length and time scales. Using (2.2) and the expressions of  $u, v$ , and  $w$  given in (2.17) we have at  $\xi = \eta = 0$ , that

$$\begin{aligned} & \frac{1}{U_\infty^2} \langle u(z, t) u(z + \zeta, t + \tau) + v(z, t) v(z + \zeta, t + \tau) + w(z, t) w(z + \zeta, t + \tau) \rangle \\ &= \iiint \int_{-\infty}^{\infty} \langle a(\alpha, \omega) a(\alpha', \omega') \rangle \frac{\delta^2}{U_\infty} \left[ \hat{u} \left( 0, \alpha \delta, \frac{\omega \delta}{U_\infty} \right) \hat{u} \left( 0, \alpha' \delta, \frac{\omega' \delta}{U_\infty} \right) \right. \\ & \quad \left. + \hat{v} \left( 0, \alpha \delta, \frac{\omega \delta}{U_\infty} \right) \hat{v} \left( 0, \alpha' \delta, \frac{\omega' \delta}{U_\infty} \right) + \hat{w} \left( 0, \alpha \delta, \frac{\omega \delta}{U_\infty} \right) \hat{w} \left( 0, \alpha' \delta, \frac{\omega' \delta}{U_\infty} \right) \right] \\ & \quad \times \exp \{ i[(\alpha + \alpha')z - (\omega + \omega')t] + i(\alpha\zeta - \omega\tau) \} d\alpha' d\omega' d\alpha d\omega = 4\pi^2 \bar{R} \delta(\zeta) \delta(\tau). \end{aligned} \tag{2.18}$$

By direct substitution (or by repeated use of Fourier transform) and normalization condition (2.15) it is straightforward to show that the solution of the integral equation (2.18) is

$$\langle a(\alpha, \omega) a(\alpha', \omega') \rangle = R \delta(\alpha + \alpha') \delta(\omega + \omega'), \tag{2.19}$$

where

$$\bar{R} = R \delta^2 / U_\infty.$$

In (2.19)  $R$  is a dimensionless number and  $\delta(\alpha + \alpha')$  and  $\delta(\omega + \omega')$  are Dirac delta-functions.

By assuming the existence of similarity and that the mean flow profile can be approximated by an error function, Townsend (1956, pp. 174–178) has shown that the turbulent Reynolds stress  $\langle uv \rangle$  at the half-velocity point of a mixing layer is equal to

$$\frac{U_\infty}{2\bar{R}x} \frac{dU}{dy},$$

where  $\bar{R} = 288$ . A good approximation of the mean velocity gradient at the half velocity point is  $\frac{1}{2}x\sigma$ . Using his measured value of the spreading parameter  $\sigma$ , Patel (1973) found that Townsend's result leads to the condition

$$\frac{\langle uv \rangle}{U_\infty^2} = 0.0096 \quad (\text{at the half-velocity point}). \tag{2.20}$$

Patel verified experimentally that (2.20) agreed quite well with his measured turbulent Reynolds stress data. Here we will use this condition to determine the remaining unknown of our model,  $R$  of equation (2.19), and thus the stochastic properties of the random amplitude function  $a(\alpha, \omega)$  are completely determined.

### 3. Second-order turbulence statistics

In this section we will use the statistical model of §2 to develop formulae for the computation of second-order turbulence statistics. We will start with single-point statistics and then discuss two-point space-time correlation functions.

#### 3.1. Single-point statistics

From equation (2.17) the autocorrelation function of the longitudinal turbulent velocity fluctuations is given by

$$\frac{\langle u(\xi, \eta, z, t) u(\xi, \eta, z, t + \tau) \rangle}{U_\infty^2} = \iiint \iiint_{-\infty}^{\infty} \langle a(\alpha, \omega) a(\alpha', \omega') \rangle \frac{\delta^2}{U_\infty} \hat{u} \left( \eta, \alpha \delta, \frac{\omega \delta}{U_\infty} \right) \hat{u} \left( \eta, \alpha' \delta, \frac{\omega' \delta}{U_\infty} \right) \times \exp \{ i[(k + k') \sigma + (\alpha + \alpha') z - (\omega + \omega') t] - i\omega \tau \} d\alpha d\alpha' d\omega d\omega', \quad (3.1)$$

where 
$$k' = k \left( \alpha' \delta, \frac{\omega' \delta}{U_\infty} \right), \quad k = k \left( \alpha \delta, \frac{\omega \delta}{U_\infty} \right).$$

Upon using (2.19) and eigenvalue and eigenfunction properties (2.13) and (2.14) we find after integrating over  $\alpha'$  and  $\omega'$

$$\frac{\langle u(\xi, \eta, z, t) u(\xi, \eta, z, t + \tau) \rangle}{U_\infty^2} = R \iint_{-\infty}^{\infty} |\hat{u}(\eta, \bar{\alpha}, \bar{\omega})|^2 \exp \left[ -2k_i \sigma - i\bar{\omega} \left( \frac{\tau U_\infty}{\delta} \right) \right] d\bar{\alpha} d\bar{\omega}. \quad (3.2)$$

By putting  $\tau = 0$  in equation (3.2) the distribution of kinetic energy associated with longitudinal turbulent velocity fluctuations is found;

$$\frac{\langle u(\xi, \eta, z, t)^2 \rangle}{U_\infty^2} = 4R \iint_0^\infty |\hat{u}(\eta, \bar{\alpha}, \bar{\omega})|^2 \exp(-2k_i \sigma) d\bar{\alpha} d\bar{\omega}. \quad (3.3)$$

The power spectrum of the kinetic energy associated with longitudinal turbulent velocity fluctuations is equal to the Fourier transform of the autocorrelation function which is given by equation (3.2). In terms of Strouhal number  $S = fx/U_\infty$  (where  $f$  is the frequency;  $f \geq 0$ ) it is straightforward to find the following formula for the power spectrum (per unit Strouhal number  $S$ ):

$$\frac{\langle u^2(\eta, S) \rangle}{U_\infty^2} = \frac{8\pi R}{\sigma} \int_0^\infty \left| \hat{u} \left( \eta, \bar{\alpha}, \frac{2\pi S}{\sigma} \right) \right|^2 \exp(-2k_i \sigma) d\bar{\alpha}. \quad (3.4)$$

By replacing  $|\hat{u}|^2$  with appropriate quantities in the above equation the autocorrelation function, power spectrum and distribution of the squares of other turbulent fluctuation quantities such as  $v$ ,  $w$ , and  $p$  can be found.

One turbulence statistic which is of particular interest and significance is the turbulent Reynolds stress  $\langle uv \rangle / U_\infty^2$ . Using (2.17) it can be computed as follows:

$$\frac{\langle u(\xi, \eta, z, t) v(\xi, \eta, z, t) \rangle}{U_\infty^2} = \frac{1}{2} \iiint \iiint_{-\infty}^{\infty} \langle a(\alpha, \omega) a(\alpha', \omega') \rangle \frac{\delta^2}{U_\infty} \times \left[ \hat{u} \left( \eta, \alpha \delta, \frac{\omega \delta}{U_\infty} \right) \hat{v} \left( \eta, \alpha' \delta, \frac{\omega' \delta}{U_\infty} \right) + \hat{u} \left( \eta, \alpha' \delta, \frac{\omega' \delta}{U_\infty} \right) \hat{v} \left( \eta, \alpha \delta, \frac{\omega \delta}{U_\infty} \right) \right] \times \exp \{ i[(k + k') \sigma + (\alpha + \alpha') z - (\omega + \omega') t] \} d\alpha' d\omega' d\alpha d\omega. \quad (3.5)$$

Substituting (2.19) into (3.5) and carrying out the integrations over  $\alpha'$  and  $\omega'$  we obtain

$$\frac{\langle uv(\eta) \rangle}{U_\infty^2} = 4R \iint_0^\infty \text{Re} \{ \hat{u}(\eta, \bar{\alpha}, \bar{\omega}) \hat{v}^*(\eta, \bar{\alpha}, \bar{\omega}) \exp(-2k_i \sigma) \} d\bar{\alpha} d\bar{\omega} \quad (3.6)$$

where  $\text{Re} \{ \} =$  the real part of.

### 3.2. Two-point space-time correlation functions

Let us now consider the two-point space-time correlation functions of longitudinal turbulent velocity fluctuations at  $(x_1, y_1, z)$  or  $(\xi, \eta_1, z)$  and  $(x_2, y_2, z + \zeta)$  or  $(\xi, \eta_2, z + \zeta)$  where  $\delta$  is equal to  $\delta_1$  and  $\delta_2$  respectively. Using the expressions (2.17) we have

$$\begin{aligned} \frac{\langle u(\xi, \eta_1, z, t) u(\xi, \eta_2, z + \zeta, t + \tau) \rangle}{U_\infty^2} &= \frac{\delta_1 \delta_2}{U_\infty} \iiint \int_{-\infty}^\infty \langle a(\alpha, \omega) a(\alpha', \omega') \rangle \\ &\times \hat{u} \left( \eta_1, \alpha \delta_1, \frac{\omega \delta_1}{U_\infty} \right) \hat{u} \left( \eta_2, \alpha' \delta_2, \frac{\omega' \delta_2}{U_\infty} \right) \exp \{ i[(k_1 + k_2) \sigma + (\alpha + \alpha') z - i(\omega + \omega') t] \} \\ &\times \exp \{ i[\alpha' \zeta - \omega' \tau] \} d\alpha d\omega d\alpha' d\omega', \end{aligned} \quad (3.7)$$

where  $k_1 = k(\alpha \delta_1, \omega \delta_1 / U_\infty)$  and  $k_2 = k(\alpha' \delta_2, \omega' \delta_2 / U_\infty)$ . Upon invoking equation (2.19) and integrating over  $\alpha$  and  $\omega$  and dropping the primes of the remaining integration variables,  $\alpha'$  and  $\omega'$ , we find

$$\begin{aligned} \frac{\langle u(\xi, \eta_1, z, t) u(\xi, \eta_2, z + \zeta, t + \tau) \rangle}{U_\infty^2} &= \frac{R \delta_1 \delta_2}{U_\infty} \iint_{-\infty}^\infty \hat{u}^* \left( \eta_1, \alpha \delta_1, \frac{\omega \delta_1}{U_\infty} \right) \hat{u} \left( \eta_2, \alpha \delta_2, \frac{\omega \delta_2}{U_\infty} \right) \\ &\times \exp \{ i[(-k_1^* + k_2) \sigma + \alpha \zeta - \omega \tau] \} d\alpha d\omega. \end{aligned} \quad (3.8)$$

To show that the right-hand side of equation (3.8) is a real function let us integrate equation (3.7) over  $\alpha'$  and  $\omega'$  instead of  $\alpha$  and  $\omega$  in the step that leads to (3.8). This gives

$$\begin{aligned} \frac{\langle u(\xi, \eta_1, z, t) u(\xi, \eta_2, z + \zeta, t + \tau) \rangle}{U_\infty^2} &= \frac{R \delta_1 \delta_2}{U_\infty} \iint_{-\infty}^\infty \hat{u} \left( \eta_1, \alpha \delta_1, \frac{\omega \delta_1}{U_\infty} \right) \hat{u}^* \left( \eta_2, \alpha \delta_2, \frac{\omega \delta_2}{U_\infty} \right) \\ &\times \exp \{ i[(k_1 - k_2^*) \sigma - \alpha \zeta + \omega \tau] \} d\alpha d\omega. \end{aligned} \quad (3.9)$$

The right-hand side of equation (3.8) and (3.9) are the complex conjugate of each other so that the expression is real.

In the next section we will use the numerical results computed according to the above formulae to compare with experimental measurements.

## 4. Numerical results and comparison with experiments

Before we study the numerical results of our statistical model we will first discuss what is the appropriate turbulent Reynolds number,  $R_T$ , to be used in equations (2.9) and (2.11). The introduction of the turbulent eddy viscosity terms in equation (2.4) is, of course, an empirical way to simulate the effect of the fine-scale turbulence on the large structures. Physically, the role of the fine-scale turbulence is to smooth out very steep local velocity gradients. This effect, however, should have an insignificant influence on the overall dynamical properties of the mixing layer turbulence.

Mathematically, it is well known that for sufficiently large turbulent Reynolds number the eddy viscosity terms of the Orr–Sommerfeld equation are unimportant as far as unstable waves of the two-dimensional mixing layers are concerned. Nevertheless, near the critical points of neutrally stable waves and damped waves the smoothing action of the fine scale turbulence is essential if discontinuous eigenfunctions are to be avoided (see Lin 1967, chap. 8). For the purpose of computing second-order turbulence statistics we note that in equations (3.2) to (3.6) the contributions of various components of the wave spectrum are weighted by the factor  $\exp[-2k_i\sigma]$ . For the most unstable wave-component this factor is approximately equal to 19.75. For damped waves this factor is less than unity. Thus the second-order statistics are dominated by the contributions from the unstable part of the wave spectrum so that they are numerically almost totally unaffected by the precise choice of the value of turbulent Reynolds number  $R_T$ .

As a start in choosing an appropriate value of  $R_T$  we note that the result of Townsend (1956, pp. 174–178) mentioned earlier gives an effective turbulent eddy viscosity  $\nu_T = U_\infty x/2\bar{R}$  ( $\bar{R} = 288$ ) at the half velocity point. The corresponding turbulent Reynolds number  $\bar{R}_T$  is  $2\bar{R}/\sigma$ . It is approximately equal to 52 for a spreading parameter  $\sigma = 11$ . This is, of course, the effective turbulent Reynolds number of both the large and small-scale turbulence of the mixing layer and is not the turbulent Reynolds number to be used. It is to be borne in mind that the turbulent Reynolds stress of the mixing layer is completely dominated by the effect of the large structure. However, this value of  $\bar{R}_T$  does give us a lower limit for  $R_T$ . We believe that a reasonable value of  $R_T$  which simulates the turbulent mixing effect of fine scale turbulence is probably a factor of 5 or 10 larger than this lower limit, say  $R_T = 500$ . To see how the choice of the value of  $R_T$  influences the eigenvalue and the various eigenfunctions  $\hat{v}$ ,  $\hat{u}$ , etc. of the Orr–Sommerfeld problem we carried out a number of numerical experiments. The results of these computations can be summarized as follows.

(1) For unstable waves ( $-k_i > 0$ ) the eigenvalue  $k$  is numerically unaffected by  $R_T$  for  $R_T \geq 300$ . The unstable waves are confined to a limited region of the  $\bar{\omega}$ ,  $\bar{\alpha}$  plane as shown in figure 6. In this figure contours of constant  $-k_i$  for the mean velocity profile given by (2.3a) in the inviscid limit, i.e.  $R_T \rightarrow \infty$ , are displayed. (Note that for the unstable and neutrally stable cases the inviscid eigenvalue problem of equations (2.11) and (2.12) yields well-behaved eigenvalue and eigenfunctions.)

(2) For  $R_T \geq 300$  the unstable eigenfunction  $\hat{v}$  is only slightly affected by  $R_T$ . A typical case is shown in figures 7 and 8. As can be seen the real part of  $\hat{v}$  is practically the same for  $R_T = 500$  as for the inviscid limit,  $R_T = \infty$ . The imaginary part of  $\hat{v}$  is on the other hand, slightly modified by finite turbulent Reynolds number effect. But  $\text{Re}\{\hat{v}\}$  is much larger than  $\text{Im}\{\hat{v}\}$  so that the overall effect of finite turbulent Reynolds number is still negligible.

From a computational point of view, enormous savings of computer time can be realized by carrying out the eigenvalue problem in the inviscid limit. Since the eigenvalues  $k$  and eigenfunctions  $\hat{v}$ ,  $\hat{p}$  are only insignificantly modified by finite turbulent Reynolds number we decide to carry out all our subsequent calculations (for unstable waves) of these quantities using the inviscid Orr–Sommerfeld or Rayleigh equation. The corresponding eigenfunctions  $\hat{u}$  and  $\hat{w}$ , are, however, computed according to equations (2.9b) and (2.9d) with a finite value of  $R_T$ . Figure 9 shows an example of the difference in Reynolds stress distribution computed in this way (inviscid  $\hat{v}$ , viscous  $\hat{u}$

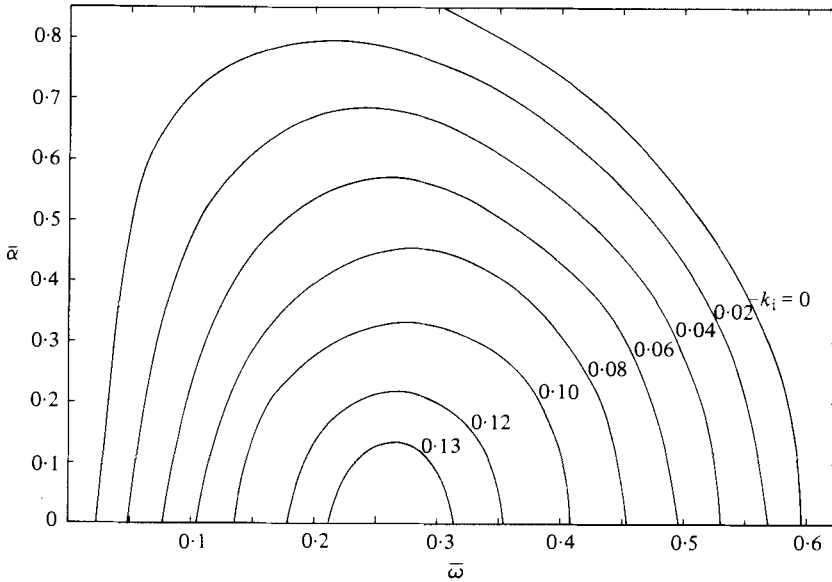


FIGURE 6. Contours of equal  $-k_i$  in the  $\bar{\omega}$ ,  $\bar{\alpha}$  plane showing the unstable region.

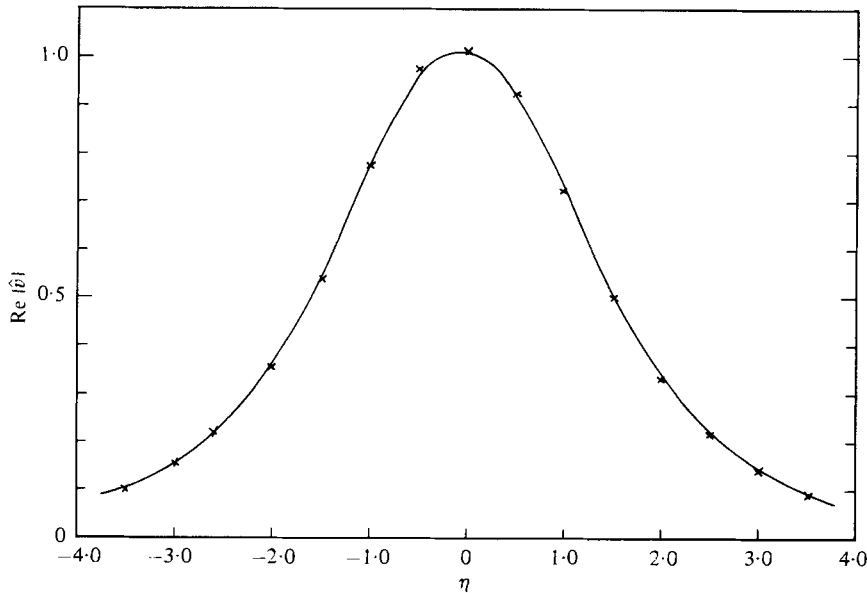


FIGURE 7. Effect of turbulent Reynolds number on the real part of the eigenfunction,  $\bar{\alpha} = 0.5$ ,  $\bar{\omega} = 0.425$ . —,  $R_T = 500$ ;  $\times - \times$ ,  $R_T = \infty$ .

with  $R_T = 500$ ) and that computed using the full Orr-Sommerfeld equation. As can be seen the overall distribution across the mixing layer remains essentially unchanged.

(3) The second-order turbulence statistics of the mixing layer as computed by the present model are insensitive to the turbulent Reynolds number used. Figures 10, 11 and 12 show typical examples of these quantities at three turbulent Reynolds

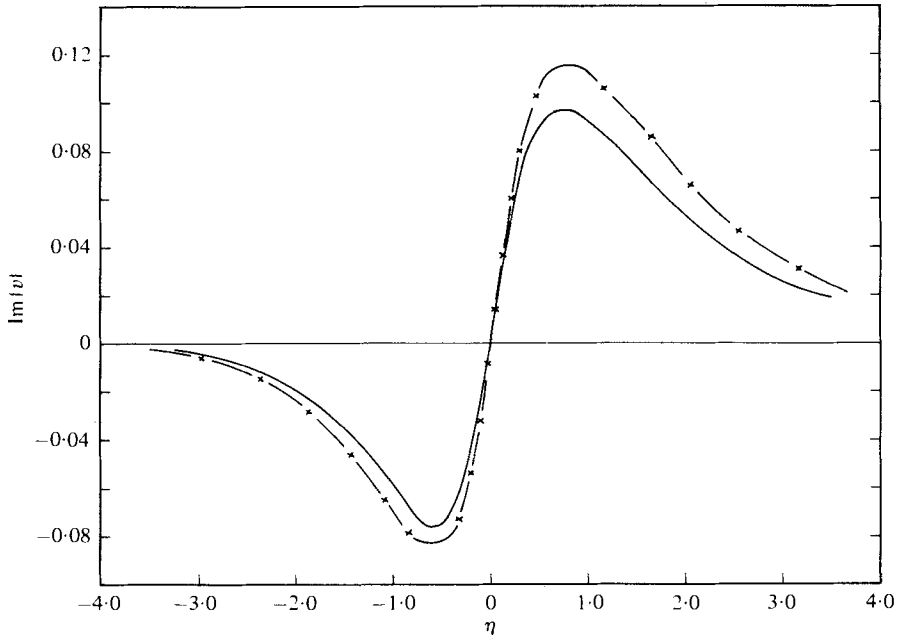


FIGURE 8. Effect of turbulent Reynolds number on the imaginary part of the eigenfunction,  $\bar{\alpha} = 0.5$ ,  $\bar{\omega} = 0.425$ . —,  $R_T = 500$ ;  $\times$ — $\times$ ,  $R_T = \infty$ .

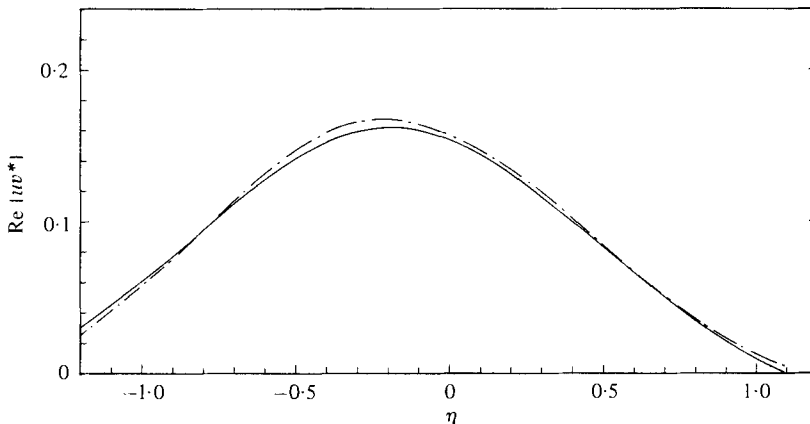


FIGURE 9. A comparison of the distributions of Reynolds stress computed using: —, the full Orr-Sommerfeld equation; ---, the Rayleigh equation for  $\hat{v}$  and  $\hat{p}$  and equation (2.9b) for  $\hat{u}$ ;  $R_T = 500$ ,  $\bar{\alpha} = 0$ ,  $\bar{\omega} = 0.105$ .

numbers;  $R_T = 150, 300$  and  $500$ . As can be seen, there is no appreciable difference between the cases  $R_T = 300$  and  $R_T = 500$  throughout the mixing layer.

(4) The damped wave components contribute an insignificant fraction to the second-order turbulence statistics.

In view of (3) above  $R_T$  is chosen to be equal to 500 in all subsequent calculations of this paper.

Before comparing our numerical results with experimental measurements we feel it is important to point out that there are noticeable differences among the measured

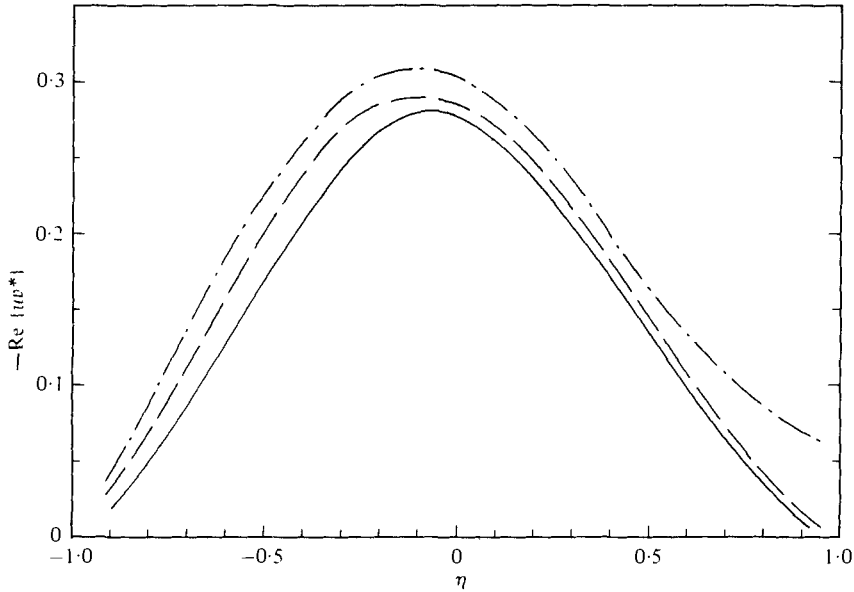


FIGURE 10. Effect of turbulent Reynolds number on  $-\text{Re}\{u u^*\}$ ;  $\bar{\alpha} = 0.2$ ,  $\bar{\omega} = 0.265$ . —,  $R_T = 500$ ; --,  $R_T = 300$ ; -·-,  $R_T = 150$ .

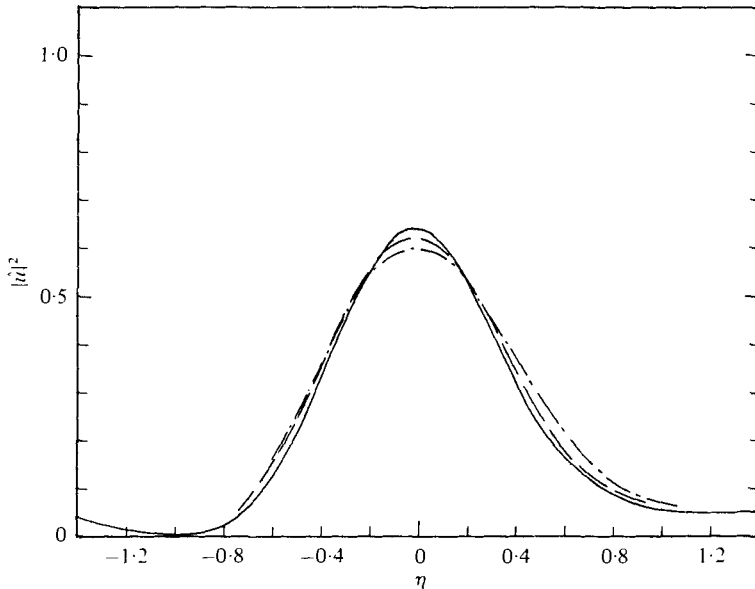


FIGURE 11. Effect of turbulent Reynolds number on  $|u'|^2$ ;  $\bar{\alpha} = 0.2$ ,  $\bar{\omega} = 0.265$ . —,  $R_T = 500$ ; --,  $R_T = 300$ ; -·-,  $R_T = 150$ .

results available in the literature. Further, the measured data are invariably restricted to single point second-order turbulence statistics. Even then, they are not complete, for the distribution of root-mean-square pressure fluctuations, an important quantity for noise prediction purposes, does not seem to have been measured at all. The first comprehensive turbulence measurements in a two-dimensional mixing layer were

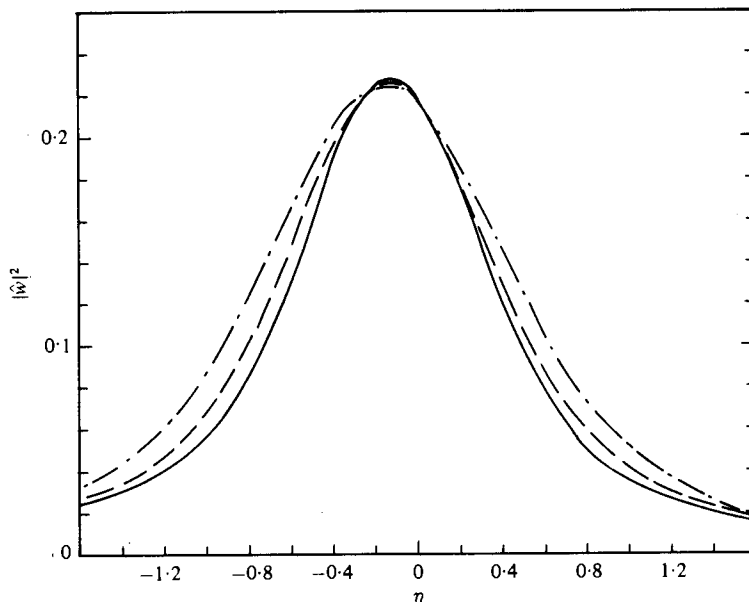


FIGURE 12. Effect of turbulent Reynolds number on  $|\hat{w}|^2$ ;  $\bar{\alpha} = 0.2$ ,  $\bar{\omega} = 0.265$ . —,  $R_T = 500$ ; --,  $R_T = 300$ ; -.-,  $R_T = 150$ .

carried out by Liepmann & Laufer (1947). Unfortunately their data are generally lower in value than those of recent experiments. Liepmann & Laufer measured the distributions of turbulent Reynolds stress  $\langle uv \rangle$ , longitudinal and transverse intensity of turbulent velocity fluctuations,  $\langle u^2 \rangle$  and  $\langle v^2 \rangle$ . However, they did not measure the lateral turbulent intensity  $\langle w^2 \rangle$ . More recently, similar experiments were performed by Wygnanski & Fiedler (1970), Patel (1973) and others. In contrast to Liepmann & Laufer, Wygnanski & Fiedler found most of these quantities to have much larger values. The measured results of Patel (1973) appears to be most reliable, at least in the sense they can be reproduced. Also they represent the largest Reynolds number results available. Champagne *et al.* (1976) repeated the two-dimensional mixing layer experiment of Patel (with a trip wire) and found remarkable agreement with his turbulence measurements. Since the measured values of Champagne *et al.* differ very little from those of Patel, for the purpose of clarity (without cluttering the figures) we will omit their data when comparing our numerical results with experiments below.

After the eigenvalues and eigenfunctions are determined the single point second-order turbulence statistics are obtained by numerical integration of the appropriate functions over the  $\bar{\omega}$ ,  $\bar{\alpha}$  plane according to the formulae given in § 3. The constant  $R$  of equation (2.19) which appears as a multiplicative factor to all second-order turbulence statistics is found by imposing condition (2.20). Its numerical value is determined to be 0.016972. Traditionally, experimental data are presented in a co-ordinate system relative to the half velocity point of the mean flow where the value of  $y$  is usually denoted as  $y_{\frac{1}{2}}$ . The half-velocity point co-ordinate  $\bar{\eta} = \sigma(y - y_{\frac{1}{2}})/x$  is related to our similarity co-ordinate  $\eta$  by a simple translation, namely,  $\bar{\eta} = \eta + 0.22$  (see figure 4). For convenience, all our results will be presented in the  $\bar{\eta}$  co-ordinate system.

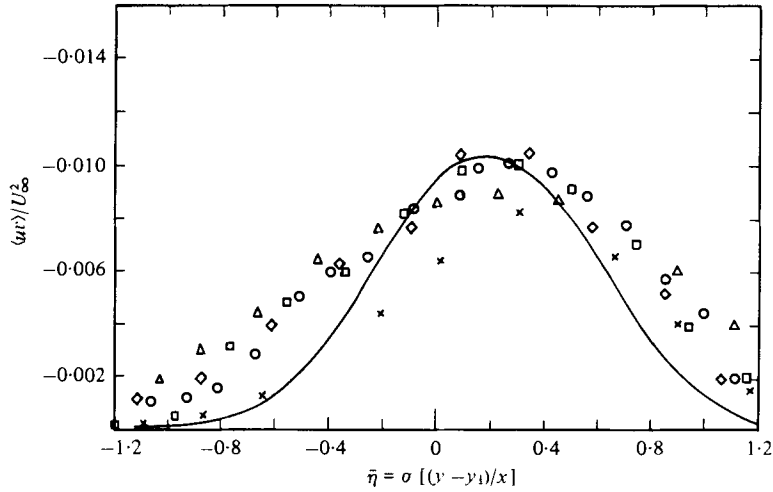


FIGURE 13. Comparison of measured and computed Reynolds stress distribution in two-dimensional mixing layers. Patel (1973):  $\diamond$ ,  $x = 28$  cm;  $\square$ ,  $x = 65.3$  cm;  $\circ$ ,  $x = 102.5$  cm.  $\Delta$ , Wygnanski & Fiedler (1970);  $\times$ , Liepmann & Laufer (1947); —, present calculation.

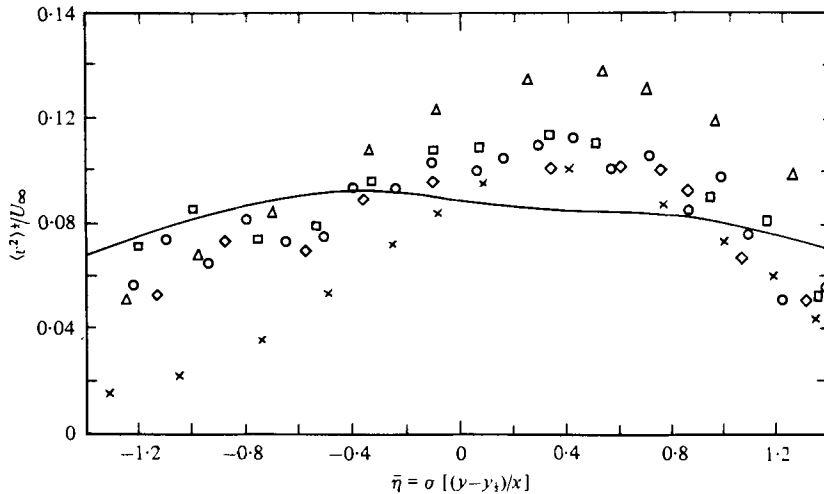


FIGURE 14. Comparison of measured and computed distribution of root-mean-square transverse turbulent velocity fluctuations. Patel (1973):  $\diamond$ ,  $x = 28$  cm;  $\square$ ,  $x = 65.3$  cm;  $\circ$ ,  $x = 102.5$  cm.  $\Delta$ , Wygnanski & Fiedler (1970);  $\times$ , Liepmann & Laufer (1947); —, present calculation.

Figure 13 shows the calculated turbulent Reynolds stress distribution  $\langle uv \rangle / U_\infty^2$  across the mixing layer. The measured data of Patel (1973), Wygnanski & Fiedler (1970) and Liepmann & Laufer (1947) are also plotted there. As can be seen the theoretical curve compares very favourably with Patel's measurements. The fact that the turbulent Reynolds stress peaks to the right, i.e. on the side of the uniform flow, of the half-velocity point is also predicted by the present statistical model.

In figures 14, 15 and 16 the calculated distributions of root-mean-square transverse, longitudinal and lateral turbulent velocity fluctuations,  $\langle v^2 \rangle^{1/2} / U_\infty$ ,  $\langle u^2 \rangle^{1/2} / U_\infty$ , and

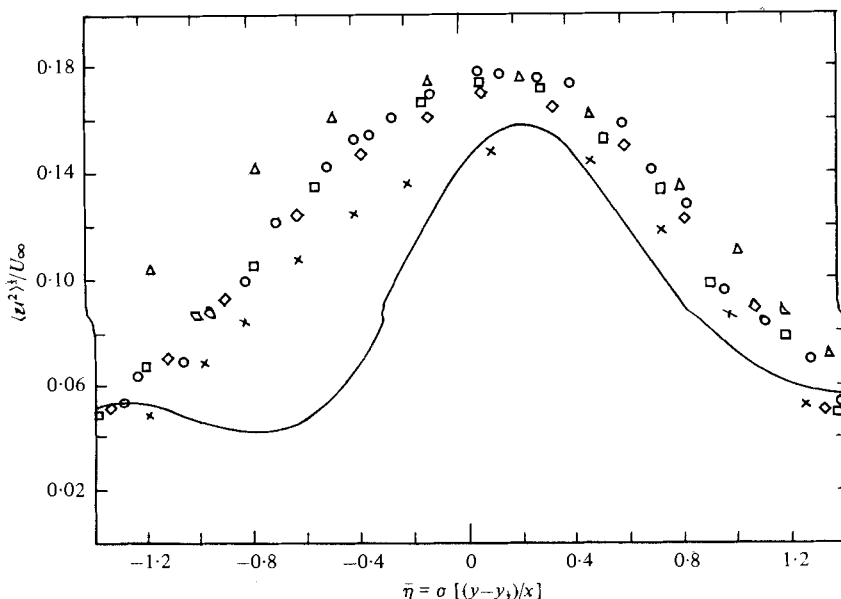


FIGURE 15. Comparison of measured and computed distribution of root-mean-square longitudinal turbulent velocity fluctuations. Patel (1973):  $\diamond$ ,  $x = 28$  cm;  $\square$ ,  $x = 65.3$ ;  $\circ$ ,  $x = 102.5$  cm.  $\triangle$ , Wygnanski & Fiedler (1970);  $\times$ , Liepmann & Laufer (1947); —, present calculation.

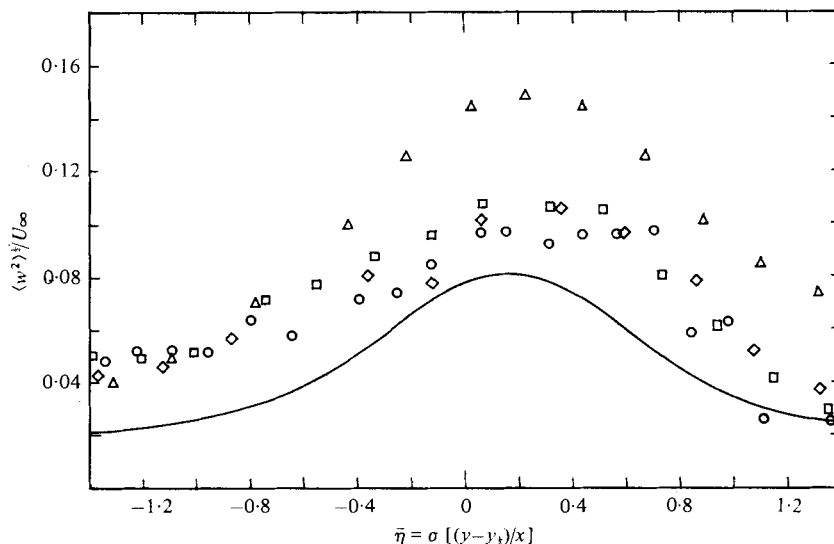


FIGURE 16. Comparison of measured and calculated distribution of root mean square lateral turbulent velocity fluctuations. Patel (1973):  $\diamond$ ,  $x = 28$  cm;  $\square$ ,  $x = 65.3$  cm;  $\circ$ ,  $x = 102.5$  cm.  $\triangle$ , Wygnanski & Fiedler (1970); —, present calculation.

$\langle w^2 \rangle^{1/2} / U_\infty$  respectively are shown together with the measured data of Patel, Wygnanski & Fiedler and Liepmann & Laufer. Considering that the present model has no adjustable constants the agreement with experimental values must be regarded as very satisfactory. Measurements indicate that the peak value of the root-mean-square longitudinal velocity fluctuations is about twice as large as that of the transverse and

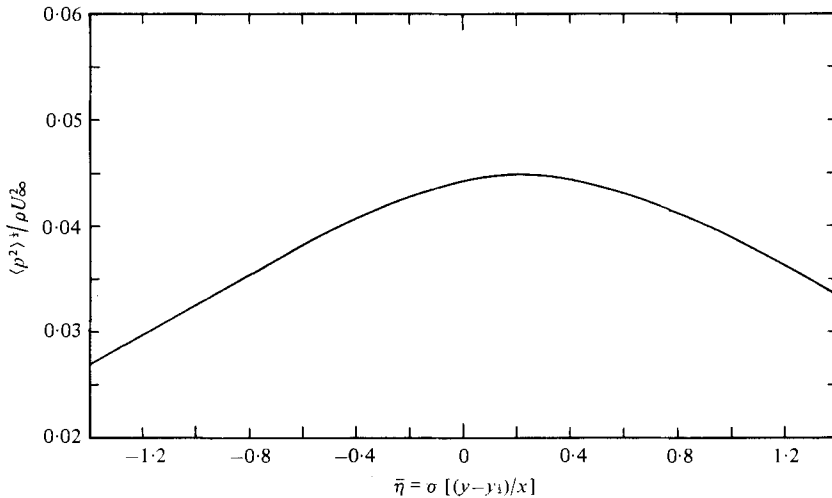


FIGURE 17. Distribution of root-mean-square pressure fluctuations across the mixing layer. (No data available in the literature for comparison.)

lateral components. This is reproduced by the model. In addition, the peak positions of the longitudinal and lateral turbulence intensity are again correctly calculated when compared with experiments. One disappointing feature, however, is the unexpected rapid drop-off of the model  $\langle u^2 \rangle^{1/2}/U_\infty$  distribution for negative values of  $\bar{\eta}$  as shown in figure 15. The cause of this discrepancy is not completely known. But it is believed that a strong contributing factor is that the simple mean velocity profile given by equation (2.3a) does not fit the real situation as well as we wish. In addition the neglect of fine-scale turbulence in our model may also be a slightly larger source of error than was anticipated.

Figure 17 shows the root-mean-square pressure distribution across the mixing layer as computed according to the present model. As far as we know no such data are available in the literature. It would be interesting if new experiments can be carried out to test this prediction.

Finally, figure 18 shows the calculated power spectrum of the longitudinal turbulent velocity fluctuations associated with the large structures of the mixing layer as a function of Strouhal number  $S = fx/U_\infty$  on the plane  $y = 0$ . The spectrum peaks at  $S \simeq 0.5$  which agrees with Laurence's measured data in the mixing layer of a jet shown in figure 3. The large structures in a jet are generally in the form of toroidal vortices. Far downstream of the nozzle exit the radii of these vortices are no longer small in comparison with the radius of curvature of the torus. As a result the large structures in a jet differ appreciably from those in a plane mixing layer. On comparing the spectrum of figure 18 and the spectra of the two axial stations closest to the nozzle exit of figure 3 remarkable agreement is found for frequencies below the peak value. The theoretical spectrum does not take into consideration the high frequency fine-scale turbulence components so that it drops off rapidly with increasing Strouhal number. This accounts for the narrowness of the calculated spectrum as compared to figure 3. Pressure fluctuation power spectra measured in the potential cone of a jet away from fine-scale turbulence by Ko & Davies (1971), however, look qualitatively

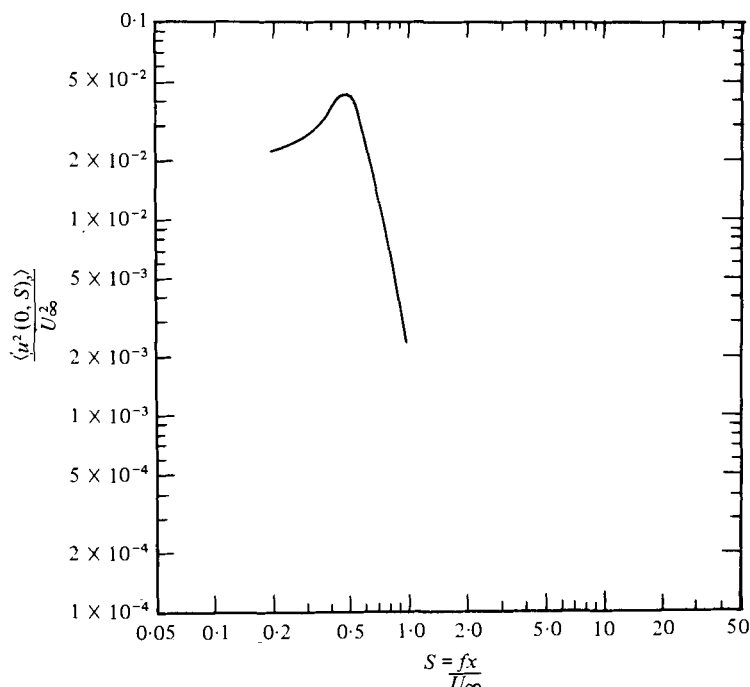


FIGURE 18. Power spectrum of longitudinal turbulent velocity fluctuations associated with the large structures of two-dimensional mixing layers on the plane  $y = 0$ .

very similar to that of figure 18. We believe these are evidence which support the contention of the present model that the power spectrum of the large structures is indeed quite narrow.

## 5. Discussion

In this paper a quasi-equilibrium statistical model capable of predicting the second-order turbulence statistics of a two-dimensional mixing layer is developed. The numerical results of this model were compared with experimental measurements. Very favourable overall agreement is found. Often the validity of a model is judged not only on the soundness of its underlying physical principles but also on how well it can predict useful physical quantities. Here we would like to point out that for the latter purpose the following factor should be taken into consideration. The present model is developed for an idealized situation somewhat removed from many of the complications encountered in a real experiment. It is well known that in a test section of finite size a two-dimensional mixing layer very rarely attains a completely fully developed turbulent state. Under this condition the measured turbulence statistics in the mixing layer is subjected to the influence of the initial condition, namely, whether the boundary layer at the trailing edge of the splitter plate is laminar or turbulent. Experimentally such effect on the development of the mean flow of mixing layers was observed by Batt (1975). The intensity of upstream disturbances too, also have some influence on a turbulent mixing layer which is not fully developed. Brad-

shaw (1966) and Chandrsuda *et al.* (1978) have investigated this phenomenon and discussed its consequences. Indeed, these factors may well be the cause of disagreements among the different sets of experimental data obtained in the past as elaborated by Champagne *et al.* (1976). The point is, because of the variability of experimental conditions, our results must be viewed as providing only a best estimate of the turbulence characteristics of fully developed two-dimensional turbulent mixing layers in laboratory conditions.

There exist presently in the literature several semi-empirical theories based on the closure approach (using averaged moment equations and turbulence transport models) which can predict certain single point second-order turbulence statistics. Some of these theories can be used to calculate distributions of turbulent Reynolds stresses, intensities of turbulent velocity components with accuracy comparable to our results. However, from a utilitarian point of view, the present statistical model may still be considered slightly superior to these theories. For as far as is known, none of these theories can provide accurate estimates of the distribution of root-mean-square pressure fluctuations. In addition, one fundamental drawback of closure approach is that, as they are, the averaged equations cannot be used to compute power spectra as well as two-point space-time correlation functions. To conclude, we believe the present statistical model is unique, at least, in these respects.

This work was supported by the NASA Langley Research Center under grant NSG-1329.

## Appendix

### *Relationship between eigenvalue and eigenfunction with positive and negative frequencies and wavenumbers*

In § 2 the normal modes of the flow are taken to be given by the solutions of the Orr-Sommerfeld equation (2.11) and boundary condition (2.12). They are

$$\left(\frac{d^2}{d\eta^2} - \bar{\alpha}^2 - k^2\right)^2 \hat{v} - iR_T \left[ (k\bar{U}_T - \bar{\omega}) \left(\frac{d^2}{d\eta^2} - \bar{\alpha}^2 - k^2\right) \hat{v} - k\bar{U}_T'' \hat{v} \right] = 0, \quad (\text{A } 1)$$

$$\hat{v} \rightarrow 0 \quad \text{as} \quad \eta \rightarrow \pm \infty. \quad (\text{A } 2)$$

For given values of  $\bar{\omega}$  and  $\bar{\alpha}$  (both are real), (A 1) and (A 2) form an eigenvalue problem. The eigenvalue is  $k$  and the eigenfunction is  $\hat{v}$ , which, in general, are complex. Now in (A 1) and (A 2) the parameter  $\bar{\alpha}$  appears as  $\bar{\alpha}^2$  so that the eigenvalue problem is invariant to the transformation  $\bar{\alpha} \rightarrow -\bar{\alpha}$ .

By taking the complex conjugate of (A 1) and (A 2) we have (\* denotes complex conjugate)

$$\left[\frac{d^2}{d\eta^2} - \bar{\alpha}^2 - (-k^*)^2\right]^2 \hat{v}^* - iR_T \left\{ [(-k^*)\bar{U}_T - (-\bar{\omega})] \left[\frac{d^2}{d\eta^2} - \bar{\alpha}^2 - (-k^*)^2\right] \hat{v}^* - (-k^*)\bar{U}_T'' \hat{v}^* \right\} = 0, \quad (\text{A } 3)$$

$$\hat{v}^* \rightarrow 0 \quad \text{as} \quad \eta \rightarrow \pm \infty. \quad (\text{A } 4)$$

On comparing (A 1) and (A 2) with (A 3) and (A 4) it is clear that if  $k(\bar{\alpha}, \bar{\omega})$  is an eigenvalue then  $k(\bar{\alpha}, -\bar{\omega}) = -k^*(\bar{\alpha}, \bar{\omega})$  is also an eigenvalue. The corresponding eigenfunction is  $\hat{v}^*(\eta, \bar{\alpha}, \bar{\omega})$  which is equal to  $\hat{v}(\eta, \bar{\alpha}, -\bar{\omega})$  if normalization condition (2.15a) is employed.

## REFERENCES

- BARK, F. H. 1975 On the wave structure of the wall region of a turbulent boundary layer. *J. Fluid Mech.* **70**, 229–250.
- BATT, R. G. 1975 Some measurements on the effect of tripping the two dimensional shear layer. *A.I.A.A. J.* **13**, 245–247.
- BRADSHAW, P. 1966 The effect of initial conditions on the development of a free shear layer. *J. Fluid Mech.* **26**, 225–236.
- BROWN, G. L. & ROSHKO, A. 1974 On density effects and large structure in turbulent mixing layers. *J. Fluid Mech.* **64**, 775–816.
- CHAMPAGNE, F. H., PAO, Y. H. & WYGNANSKI, I. J. 1976 On the two dimensional mixing region. *J. Fluid Mech.* **74**, 209–250.
- CHAN, Y. Y. 1974*a* Spatial waves in turbulent jets. *Phys. Fluids* **17**, 46–53.
- CHAN, Y. Y. 1974*b* Spatial waves in turbulent jets. Part II. *Phys. Fluids* **17**, 1667–1670.
- CHAN, Y. Y. 1976 Spatial waves of higher modes in an axisymmetric turbulent jet. *Phys. Fluids* **19**, 2042–2043.
- CHAN, Y. Y. 1977 Wavelike eddies in a turbulent jet. *A.I.A.A. J.* **15**, 992–1001.
- CHANDRUSUDA, C., MEHTA, R. D., WEIR, A. D. & BRADSHAW, P. 1978 Effect of free-stream turbulence on large structures in turbulent mixing layers. *J. Fluid Mech.* **85**, 693–704.
- DIMOTAKIS, P. E. & BROWN, G. J. 1976 The mixing layer at high Reynolds number: Large-structure dynamics and entrainment. *J. Fluid Mech.* **78**, 535–560.
- KO, N. W. M. & DAVIES, P. O. A. L. 1971 The near field within the potential cone of subsonic cold jets. *J. Fluid Mech.* **50**, 49–71.
- LANDAHL, M. 1967 A wave-guide model for turbulent shear flow. *J. Fluid Mech.* **29**, 441–459.
- LANDAHL, M. 1975 Wave breakdown and turbulence. *SIAM J. Appl. Mech.* **28**, 735–756.
- LAURENCE, J. C. 1956 Intensity, scale and spectra of turbulence in mixing regions of free subsonic jets. *N.A.C.A. Rep.* 1292.
- LIEPMANN, H. & LAUFER, J. 1947 Investigations of free turbulent mixing. *N.A.C.A. Tech. Note* 1257.
- LIN, C. C. 1967 *Theory of Hydrodynamic Stability*. Cambridge University Press.
- MALKUS, W. V. R. 1956 Outline of a theory of turbulent shear flow. *J. Fluid Mech.* **1**, 521–539.
- MOORE, C. J. 1977 The role of shear layer instability waves in jet exhaust noise. *J. Fluid Mech.* **80**, 321–367.
- PATEL, R. P. 1973 An experimental study of a plane mixing layer. *A.I.A.A. J.* **11**, 67–71.
- ROSHKO, A. 1976 Structure of turbulent shear flows: A new look. *A.I.A.A. J.* **14**, 1349–1357.
- TOWNSEND, A. A. 1956 *The Structure of Turbulent Shear Flow*. Cambridge University Press.
- WINANT, C. D. & BROWAND, F. K. 1974 Vortex pairing: the mechanism of turbulent mixing layer growth at moderate Reynolds numbers. *J. Fluid Mech.* **63**, 237–255.
- WYGNANSKI, I. & FIEDLER, H. E. 1970 The two-dimensional mixing region. *J. Fluid Mech.* **41**, 327–361.